electronics

MDPI

Article

Operation Features of a Coaxial Virtual Cathode Oscillator Emitting Electrons in the Outer Radial Direction

Se-Hoon Kim, Chang-Jin Lee, Wan-Il Kim and Kwang-Cheol Ko *

Department of Electrical Engineering, Hanyang University, 222, Wangsimni-ro, Seongdong-gu, Seoul 04763, Korea; d.sehoon.kim@gmail.com (S.-H.K.); jincalibur@naver.com (C.-J.L.); wanilgg@naver.com (W.-I.K.)

* Correspondence: kwang@hanyang.ac.kr

Abstract: The operation features of the coaxial virtual cathode oscillator emitting electrons in the outer radial direction were investigated through simulations and experiments. A coaxial vircator was compared with an axial vircator when the anode to cathode distance of both vircators was 6 mm. The proposed coaxial vircator was operated when the anode to cathode distance was 5 mm, 6 mm, and 7 mm. The peak power and frequency of the microwave generated from the proposed coaxial vircator when the anode to cathode distance was 6 mm were 20.18 MW and 6.17 GHz, respectively. The simulations and experiments show that the proposed coaxial vircator generates 80% more microwave power than the axial vircator with the same anode to cathode distance. According to the simulations and experiments, the proposed coaxial vircator tends to generate a higher power average when the anode to cathode distance was larger than 5 mm. The frequency of the proposed coaxial vircator when the anode to cathode distance was 5 mm and 7 mm was approximately 8 GHz and 5 GHz, respectively. The geometric factor of the proposed coaxial vircator was considered to be the reason for the greater microwave power generation than the axial vircator. The frequency of the proposed coaxial vircator decreases inversely proportional with the anode to cathode distance as observed in the axial and basic coaxial vircators.

Keywords: high-power microwave source; virtual cathode oscillator; vircator; coaxial vircator; PFN–Marx generator

Citation: Kim, S.-H.; Lee, C.-J.; Kim, W.-I.; Ko, K.-C. Operation Features of a Coaxial Virtual Cathode Oscillator Emitting Electrons in the Outer Radial Direction. *Electronics* **2022**, *11*, 82. https://doi.org/10.3390/electronics11010082

Academic Editor: Bor-Ren Lin

Received: 26 November 2021
Accepted: 27 December 2021
Published: 28 December 2021

1. Introduction

High-power microwave (HPM) devices have been investigated experimentally and numerically for use in many industrial and academic fields [1]. The use of a pulsed power source in conventional vacuum electronic devices generates microwaves from a few MW to a few GW. As the pulsed power system progresses, the HPM devices applications expand from military purposes to industrial applications. Various high-power microwave sources, such as a relativistic klystron, a relativistic magnetron, and a gyrotron, have been studied and analyzed experimentally and numerically [2–5]. Although the HPM sources have different microwave generation mechanisms, the devices were studied to modulate their microwave frequency and mode to generate microwaves with higher power and higher efficiencies. The operation features of the HPM systems have been improving through both pulsed power sources and HPM sources. Pulsed power sources have been studied to improve the impedance matching problem and resolve the microwave chirping issues caused due to the input pulse length. On the other hand, HPM sources have been investigated to improve its efficiencies by changing and optimizing its internal structures.

A virtual cathode oscillator (vircator) is a microwave source for generating HPM using space charge effects [1,6]. A vircator generates microwaves through two mechanisms: the reciprocating motion of electrons between the cathode surface and virtual cathode in the drift region, and the oscillation of the virtual cathode itself. The output frequency of the

vircator is determined by which motion is the main mechanism. Two vircator frequencies are shown as:

$$f_{vc}(\mathrm{GHz}) = \frac{5}{6\pi \times 10^7}\sqrt{\frac{eV}{md^2}} \quad (1)$$

$$f_r(\mathrm{GHz}) = \frac{9.4\sqrt{\mathrm{V(MV)}}}{d}. \quad (2)$$

Here, f_{vc} is the frequency of the virtual cathode, f_r is the frequency of the reciprocating motion, e is the electron charge, m is the electron mass, d is the anode to cathode distance in centimeters, and V is the diode voltage [7]. Unlike most microwave devices, the vircator can be driven without external magnetic field generating devices. These allow the vircator to have simple operation features, simple structure, compactness, and facile high-voltage operation. However, the vircator has relatively low efficiencies (typically ≈5%) compared with other HPM devices. A vircator is widely investigated in academic fields to improve its low efficiencies and modulate its output frequency by installing additional structures and changing the cathode and anode materials [8–16].

Various types of vircators were studied to improve the shortcomings of the most typical type, an axial vircator. A coaxial vircator is a modified version of the vircator to improve its low efficiencies [17]. Most coaxial vircators are designed to install the cathode outside the cylindrical anode and emit electrons in an inner radial direction [17–28]. The brief summarizations on the performances of other works are shown in Table 1. In this paper, a coaxial virtual cathode oscillator emitting electrons in an outer radial direction was designed and experimentally investigated. Unlike most coaxial vircators, the cathode is installed inside the cylindrical mesh anode. The coaxial vircator is driven using a 10-stage PFN–Marx generator. The operation features of the coaxial cathode were analyzed through PIC simulations and experiments for different cathode to anode distances. The microwave power and frequency of the coaxial vircator were investigated by comparing with the power and frequency of the axial vircator with the same anode to cathode distance.

Table 1. Summarization of other works on the coaxial vircator.

Direction of Electron Emission	Specification of Pulsed Power Source	Operating Frequency (GHz)	Output Power (MW)	Analysis Method	Reference Number
Inner	-	-	-	Simulations Only	[18,21,22,24]
Inner	400–1000 kV	2–6.6	Not shown	Experiments Only	[19,23,26,27]
Inner	500 kV, 40 kA	2	400	Simulations, Experiments	[17]
Inner	600 kV, 88 kA	5.47	244	Simulations, Experiments	[20]
Inner	600 kV, 50 kA	2–2.3	800	Simulations, Experiments	[25]
Outer	-	-	-	Simulations Only	[28]

2. System Description

An experimental system was designed and used to investigate the coaxial vircator. Figure 1 shows the schematic diagram of the high-power microwave system comprising three parts: a pulsed power system (10-stage PFN–Marx generator), a high-power microwave device (coaxial vircator), and a measurement system. Additional measuring devices were installed in the pulsed power system and microwave measurement system. The distance between the microwave measurement system and HPM-generating device was established considering far-field criteria.

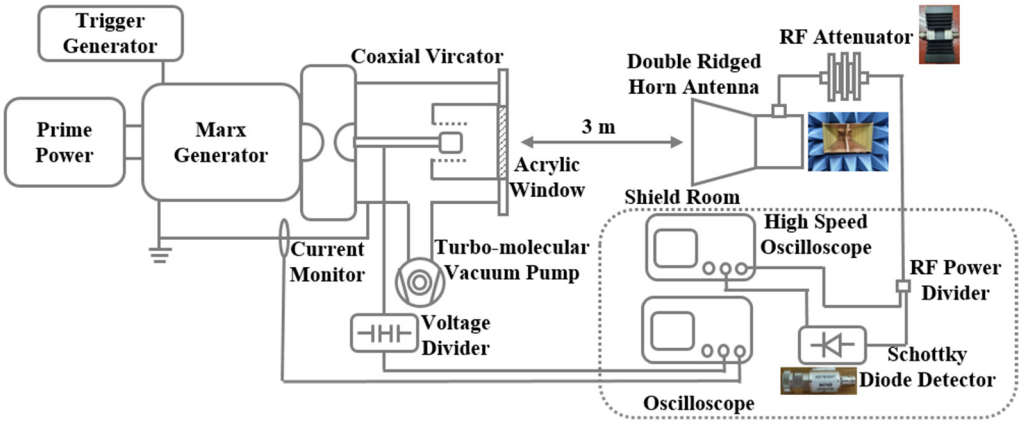

Figure 1. Schematic diagram of the experimental HPM system.

2.1. PFN–Marx Generator

Microwave devices require a high voltage to generate a high-power microwave. In most cases, a pulsed power source is used as the high-voltage source. A Pulse Forming Network (PFN)–Marx generator is a pulsed power source to operate HPM devices [12,29–31]. The PFN–Marx generator generates and applies a rectangular high-voltage pulse into the designated load without an additional pulse-forming stage. The impedance of the PFN–Marx generator can be matched to the load impedance by properly selecting the inductance and capacitance used in the generator. As a result, the PFN–Marx generator was suitable for the compact HPM system and loads with relatively low characteristic impedance such as a vircator. In this research, a 10-stage PFN–Marx generator was used to drive the proposed coaxial vircator. Each stage comprised two arrays of PFN with a characteristic impedance of 6 Ω in parallel to make the characteristic impedance of the PFN module 3 Ω. The resulting characteristic impedance of the 10-stage PFN–Marx generator was 30 Ω. The parameters of the 10-stage PFN–Marx generator are shown in Table 2. Figure 2 depicts the circuit diagram of the 10-stage PFN–Marx generator. The 10-stage PFN–Marx generator is designed to achieve −150 kV at the plateau of the voltage pulse. Each PFN module was charged negatively to −30 kV to achieve an erected voltage of −300 kV, and the PFN–Marx generator applies a plateau voltage of −150 kV to the matched load. Figure 3 shows the experimental waveform of the PFN–Marx generator. Although the impedance was not exactly matched, the 10-stage PFN–Marx generator achieves the peak voltage of −195 kV, and the plateau voltage was approximately −150 kV.

Table 2. Design parameters of the 10-stage PFN–Marx generator.

Quantity	Value	Quantity	Value
Capacitance	2.08 nF	Inductance	75 nH
PFN stage	6	Marx stage	10
Charging voltage	−30 kV	Erected voltage	−300 kV
Pulse width	150 ns	Characteristic impedance	30 Ω

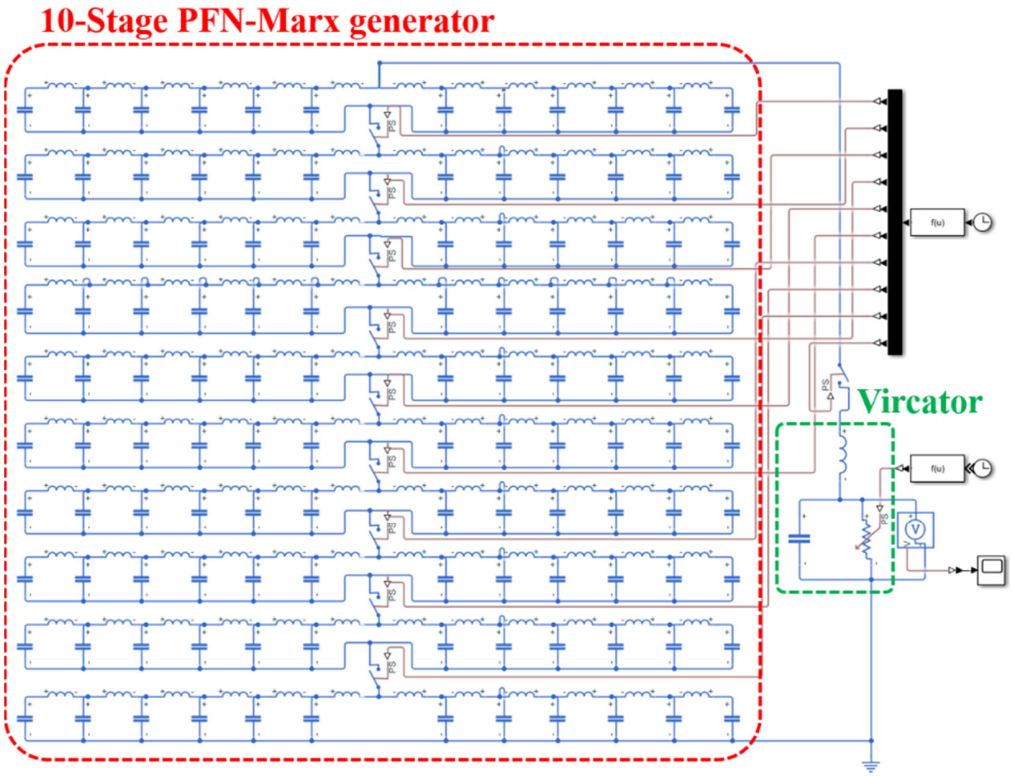

Figure 2. Circuit diagram of the 10-stage PFN-Marx generator.

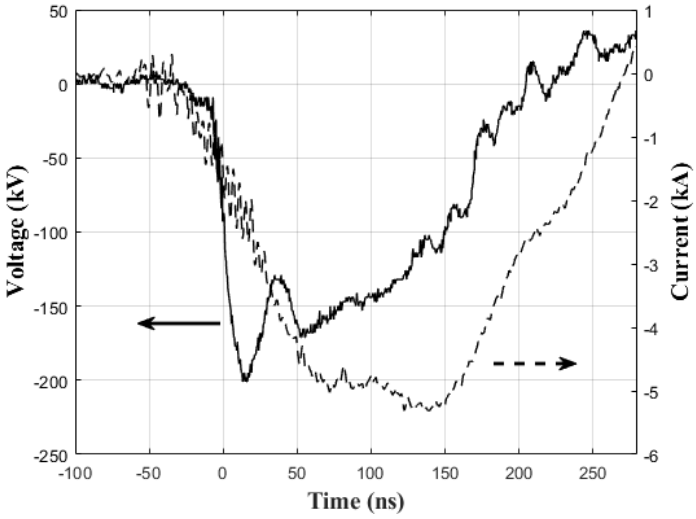

Figure 3. Typical output waveform of the diode voltage and diode current applied to the proposed coaxial vircator (D_{AK} = 6 mm).

2.2. Coaxial Vircator

Figure 4 shows the inner structure of the proposed coaxial vircator. A stainless-steel vacuum chamber (300 mm in diameter and 400 mm in length) enclosed the coaxial vircator. A drift tube with a diameter of 200 mm was installed inside the vacuum chamber to attach the coaxial structure assemblies. The vacuum chamber was evacuated using a turbo-molecular vacuum pump. During the experiments, the inner pressure was maintained between 2×10^{-5} torr and 3×10^{-5} torr. A cathode holder and a back-plate of the vacuum chamber were fabricated using a poly-ether-ether ketone (PEEK) to provide electrical insulation between the chamber and voltage feeder. A cylindrical stainless-steel mesh anode with geometric transparency of 70% and a graphite cathode were used as a vircator

diode. The inner diameter and length of the mesh anode were 82 mm and 110 mm, respectively. Cathodes with a length of 30 mm were used in simulations and experiments. The coaxial vircator was investigated when the anode to cathode distance was 5 mm, 6 mm, and 7 mm. The anode to cathode distance was adjusted by changing the cathode's diameter. The design parameters of the proposed vircator diode are shown in Table 3.

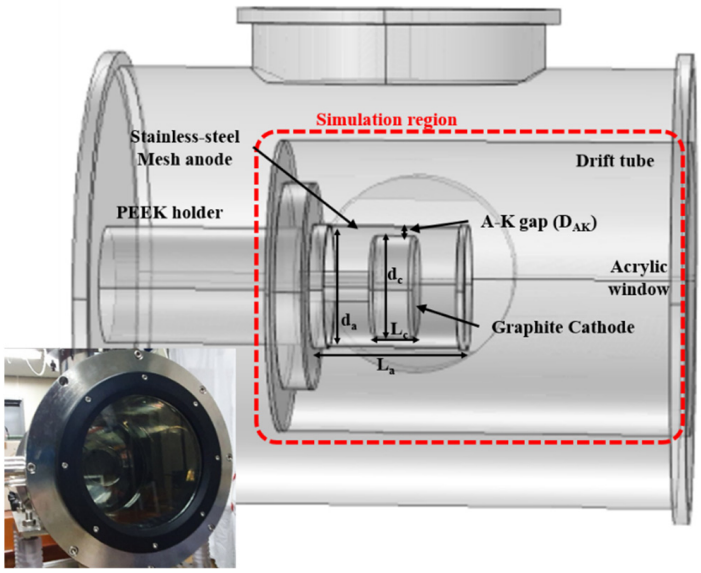

Figure 4. Inner structure of the coaxial vircator.

Table 3. Design parameters of the proposed coaxial vircator diode.

Quantity	Value	Quantity	Value
Cathode length (L_c)	30 mm	Cathode diameter (d_c)	68, 70, 72 mm
Anode length (L_a)	110 mm	Anode diameter (d_a)	82 mm
Anode transparency	70%		

2.3. Measurement Equipment

The characteristics of the pulsed power system were required to analyze the operation features of the coaxial vircator. The voltage and current applied to the coaxial vircator diode were measured using a capacitive voltage divider and a Pearson coil, respectively. Both the capacitive voltage divider and Pearson coil were installed in the voltage feed-through covered in the PEEK holder. An oscilloscope (DPO 3054, Tektronix) was used to record the waveform from the voltage divider and current monitor.

A double-ridged horn antenna was installed 3 m apart from the vircator window to measure the generated microwave power. The received microwave power from the vircator was converted into voltage using a planar-doped barrier diode detector (8474B, Keysight Technologies). A high-speed oscilloscope (MSO 71604C, Tektronix) was used to record the microwave signal and diode detector output. A −30 dB attenuator was installed after the horn antenna to protect the recording oscilloscope and diode detector. Considering the attenuation at the measurement cable and the insertion loss at the power divider, the overall attenuation at the microwave measurement system was −51 dB. A fast Fourier transform (FFT) was used to calculate the microwave frequency from the directly applied microwave signal into the high-speed oscilloscope.

The microwave power from the coaxial vircator was calculated using Friis's equation, which is given as:

$$P_t = \frac{P_r}{G_t G_r}\left(\frac{4\pi D}{\lambda}\right)^2 \quad (3)$$

where P_t is the power at the transmitting antenna, P_r is the power at the receiving antenna, G_t is the transmitting antenna gain, G_r is the receiving antenna gain, D is the distance between the transmitting receiving antenna, and λ is the wavelength of the microwave signal [24]. The gain of the transmitting antenna (G_t) and the gain of the double-ridged horn antenna (G_r), which are used in calculating Friis's equation, were 18.5 dBi and 12.82 dBi, respectively.

3. PIC Simulation and Experimental Results

The operation features of the coaxial vircator emitting electrons in the outer radial direction were investigated through PIC simulations and experiments. First, the coaxial vircator was analyzed by comparing the microwave power and frequency with that of the axial vircator. Second, the microwave power and frequency of the coaxial vircator were measured and analyzed when the anode to cathode distance was 5 mm, 6 mm, and 7 mm to observe the influence of the anode to cathode distance on the vircator operations.

3.1. PIC Simulation

The axial vircator and proposed coaxial vircator were analyzed using an FDTD-PIC (Finite-Difference-Time-Domain Particle-In-Cell) simulation (CST particle studio). The drift tube excluding the rest vircator chamber was modeled as the main simulation region. The simulation region used in the PIC simulation is shown in Figure 4. The diameter and length of the simulation region were 200 mm and 300 mm, respectively. In the case of the axial vircator, a disk-shaped thin sheet anode was placed 6 mm after the cathode surface. A cylindrical cathode with a radius of 35 mm and a length of 30 mm was placed at z = 20 mm. For the proposed coaxial vircator, a cylindrical sheet with a radius of 41 mm and a length of 110 mm was used as the transparent anode. A cylindrical cathode with the same specification as the axial vircator was placed at z = 50 mm. All of the vircator structures were modeled as a perfect electric conductor. The anode to cathode distance of the proposed coaxial vircator was controlled through the cathode radius. In simulations, the transparency of both the disk-shaped and cylindrical sheet anode was set to 70%. The electron-emitting threshold voltage was set to 100 kV/m. The vircators were simulated using a ramp-shaped voltage pulse with a pulse width of 25 ns and a plateau voltage of 150 kV.

Figure 5 shows the typical phase diagram of the axial vircator and proposed coaxial vircator with an anode to cathode distance (D_{AK}) of 6 mm. The phase diagram of the axial vircator and proposed coaxial vircator was plotted along the z-axis and the x-axis, respectively. The direction of the axis represents the direction of the electron emission for each type of vircator. Since the electrons were emitted in every radial direction, the phase diagram of the proposed coaxial vircator had symmetric figures along the x-axis. Figure 6 shows the 2D electron energy distribution plot on the proposed coaxial vircator. The virtual cathode was formed across the sheet anode and spread along the sheet anode in the direction of the z-axis. The shape of the virtual cathode was an effect of the electron path between the virtual cathode and cathode surface. The excitation mode was TM_{01}. The transverse magnetic mode propagated at 5.85 GHz.

The simulation results of the microwave power from the vircators are depicted in Figure 7. The microwave power from the proposed coaxial vircator was normalized using the power from the axial vircator. According to the simulations, the proposed coaxial vircator enhances the microwave power by up to 190% when the anode to cathode distance was 7 mm. Additionally, the microwave power enhancement dramatically increased when the anode to cathode distance was varied from 5 to 6 mm. The frequency of the generated microwave power was calculated through FFT. The frequency spectra of the axial and proposed coaxial vircator with the different anode to cathode distance are shown in Figure 8. Although the input voltage and anode to cathode distance are the same, the frequency was expected to be different because of the difference between the geometric factor of the axial vircator and proposed coaxial vircator. However, the dominant frequency

of the axial and proposed coaxial vircator with the anode to cathode distance of 6 mm was approximately 5.9 GHz. The dominant frequency of the proposed coaxial vircator decreased as the anode to cathode distance increased. As observed in the axial vircator and normal coaxial vircator [27,32], the inversely proportional tendency of the dominant frequency and anode to cathode distance was also observed in the proposed coaxial vircator. According to the equations on the vircator frequency, the reciprocating motion of electrons between the cathode and virtual cathode was the principle microwave generation of both the axial and proposed vircators. Unlike the axial vircator with single peaks shown in the frequency spectra, the frequency spectrum of the proposed coaxial vircator had several peaks. As shown in Figure 6, the proposed coaxial vircator had a broader virtual cathode along the mesh anode. The distribution of the virtual cathode caused the peaks of the proposed coaxial vircator.

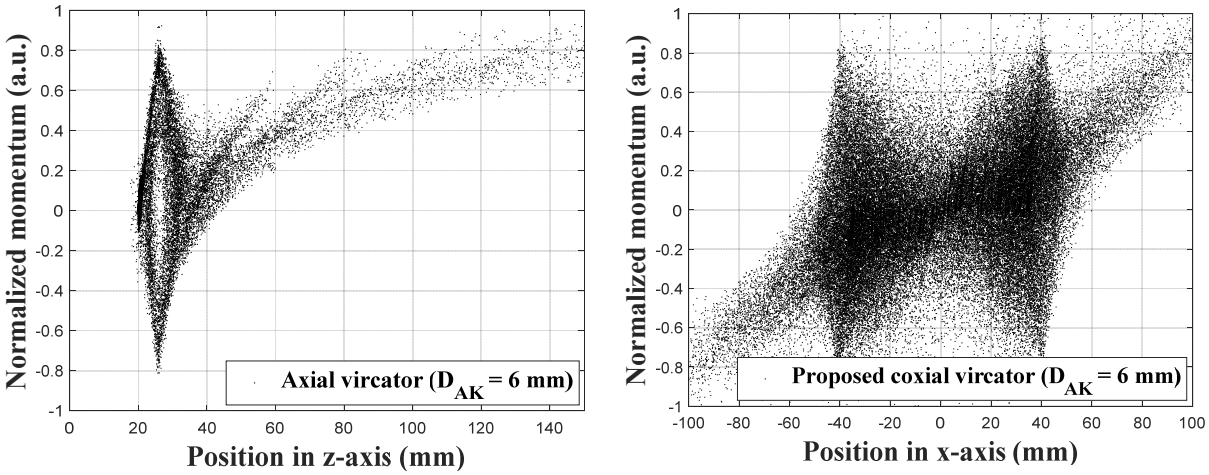

(**a**) Axial vircator (**b**) Proposed coaxial vircator

Figure 5. Phase space diagram of the axial and proposed coaxial vircator (D_{AK} = 6 mm).

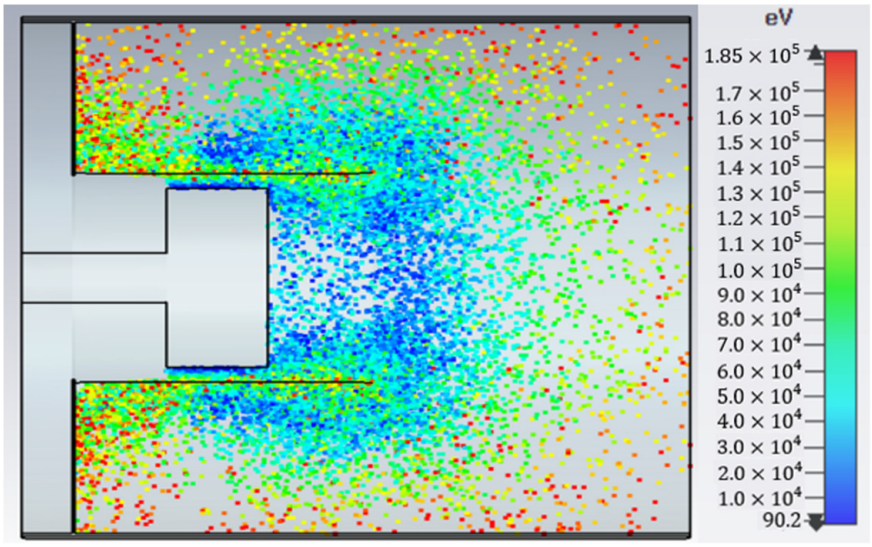

Figure 6. Two-dimensional (2D) electron energy distribution plot on the proposed coaxial vircator (D_{AK} = 6 mm).

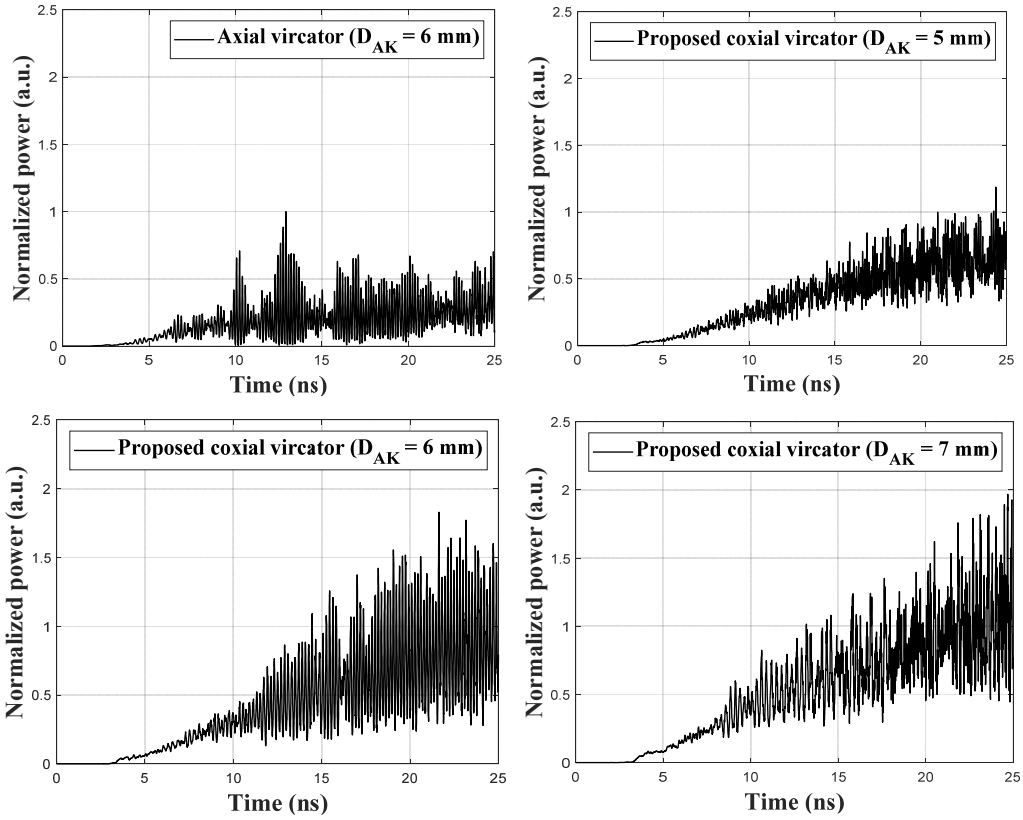

Figure 7. Normalized microwave power of the axial vircator and proposed coaxial vircator.

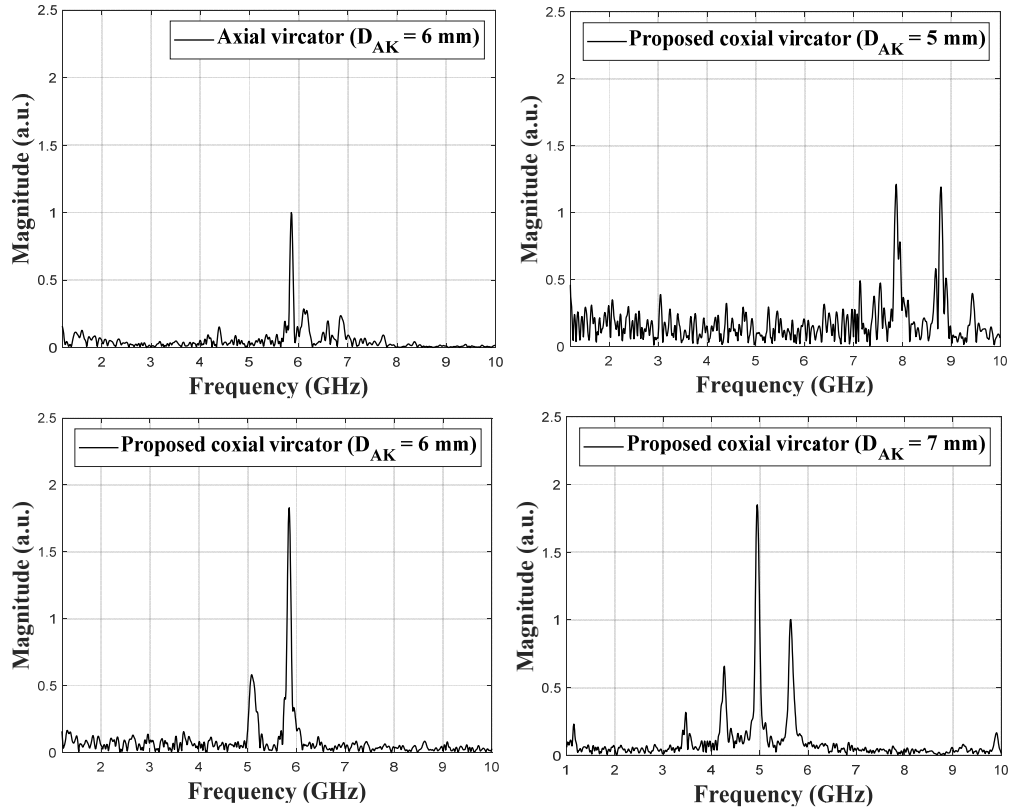

Figure 8. Frequency spectrum of the axial vircator and proposed coaxial vircator.

3.2. Experimental Results

The coaxial vircator emitting electrons in the outer radial direction was investigated to analyze its operation features when its anode to cathode distance was 5 mm, 6 mm, and 7 mm. The typical voltage and current waveforms for the proposed coaxial vircator when the anode to cathode distance was 6 mm are shown in Figure 3. The measured peak and plateau diode voltage were -201 ± 5 kV and -153 ± 7 kV, respectively. The rise time and pulse width of the voltage pulse were approximately 23 ns and 200 ns, respectively. The diode current was -5.58 ± 0.3 kA. Although the change in the vircator type and anode to cathode distance affects the diode impedance, the variation in the plateau diode voltage and diode current is within ∓ 15 kV and ± 1.5 kA, respectively. The output microwave power from the vircators were calculated using the voltage from the RF diode detector. The dominant frequencies were calculated through the FFT of the recorded microwave. The typical RF diode detector voltage waveforms for the axial and proposed coaxial vircator when the anode to cathode distance was 6 mm are shown in Figure 9. In both cases, the microwaves were generated for approximately 140 ns, which was slightly shorter than the pulse width of the diode voltage. Figure 10 shows the typical frequency spectrum of the radiated microwave from the axial and proposed coaxial vircator when the anode to cathode distance was 6 mm. As shown in the typical plots, the proposed coaxial vircator tends to have several smaller peaks in addition to the dominant frequency than the axial vircator. However, the proposed coaxial vircator tends to be sharper near the dominant frequencies than the axial vircator. The complete experimental results are shown in Table 4. The maximum values of the measured microwave power were 10% to 23% greater than the average value. The minimum values of the measured microwave power were 11% to 22% less than the average. The deviation of the microwave power was greatest when the proposed coaxial cathode was operated and the anode to cathode distance was 5 mm.

The microwave power results from the vircators were normalized using the microwave power from the axial vircator to compare the simulation results and experimental results. The normalized microwave powers on the axial vircator and coaxial vircator with the different anode to cathode distances were plotted in Figure 11. When the anode to cathode distance was 6 mm, the proposed coaxial vircator generates microwave power 80% greater than that of the axial vircator. As shown in both simulations and experiments, the generated microwave power from the proposed coaxial vircator increased dramatically when the anode to cathode distance varied from 5 to 6 mm. Although the experimental results show differences for 5 mm and 7 mm, the proposed coaxial vircator enhances microwave power in a tendency analogous to the simulations. The difference for 5 mm and 7 mm was caused by the misalignment of the anode and mesh anode, the crumpled condition of the mesh anode, and the difference between the diode voltage of the simulation and experiments. Figure 12 shows the dominant frequency of the simulations and the experiments. The experimental results on the dominant frequency were analogous to the simulation results. The dominant frequency of the proposed coaxial vircator decreased inversely proportional to the anode to cathode distance, as observed in the axial vircator and normal coaxial vircator. The small difference in frequency of the simulations and experiments is because of the diode voltage and anode to cathode distance. Although the geometric factor affects the vircator frequency, the diode voltage and anode to cathode distance is the major factor deciding the frequency. Unlike the simulations, the diode voltage in the experiments was not exactly 150 kV, and the anode to cathode distance was slightly changed because the mesh anode was not a perfect cylinder.

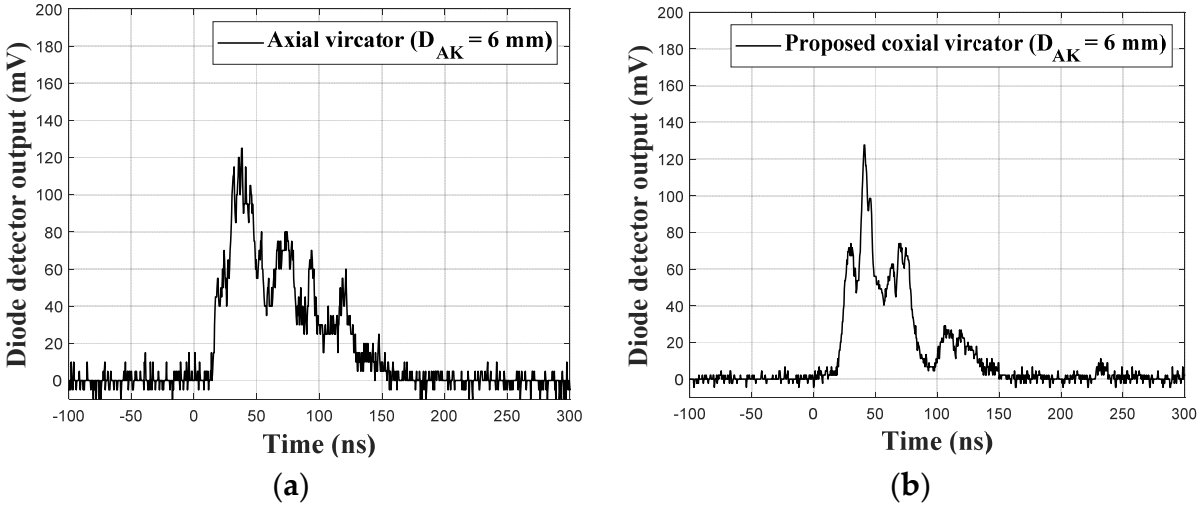

Figure 9. Typical diode detector output waveform of the vircator (D_{AK} = 6 mm): (**a**) axial vircator and (**b**) coaxial vircator.

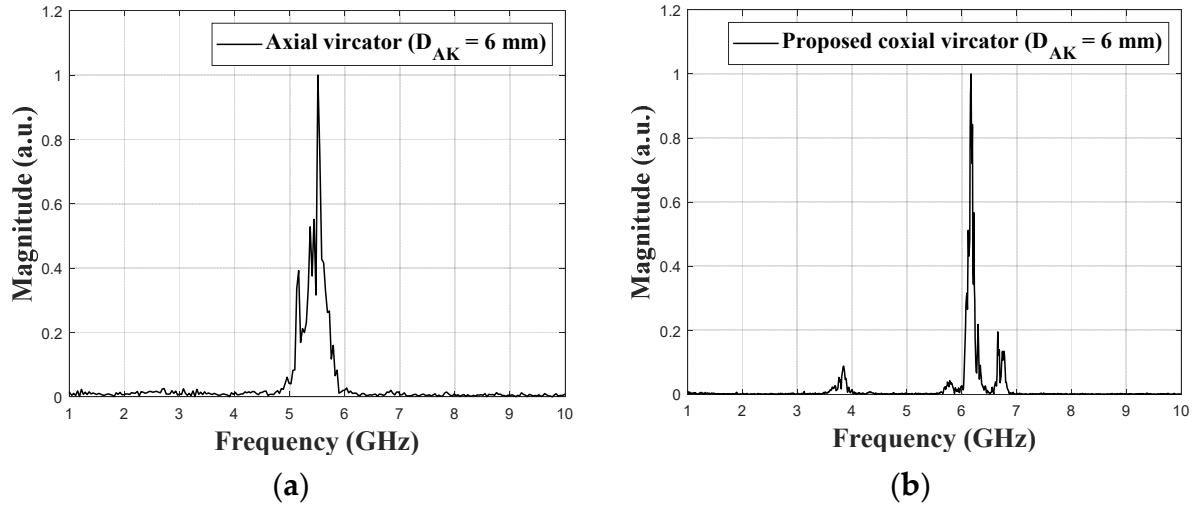

Figure 10. Typical frequency spectrum of the vircator (D_{A-K} = 6 mm): (**a**) axial vircator and (**b**) coaxial vircator.

Table 4. Experimental results on the vircator.

D_{A-K}	P_{min} (MW)	P_{max} (MW)	P_{avg} (MW)	Frequency (GHz)
Axial (6 mm)	8.7	12.3	11.22	5.54
5 mm	8.87	13.3	10.76	8.05
6 mm	17.99	22.65	20.18	6.17
7 mm	14.93	19.36	17.26	5.12

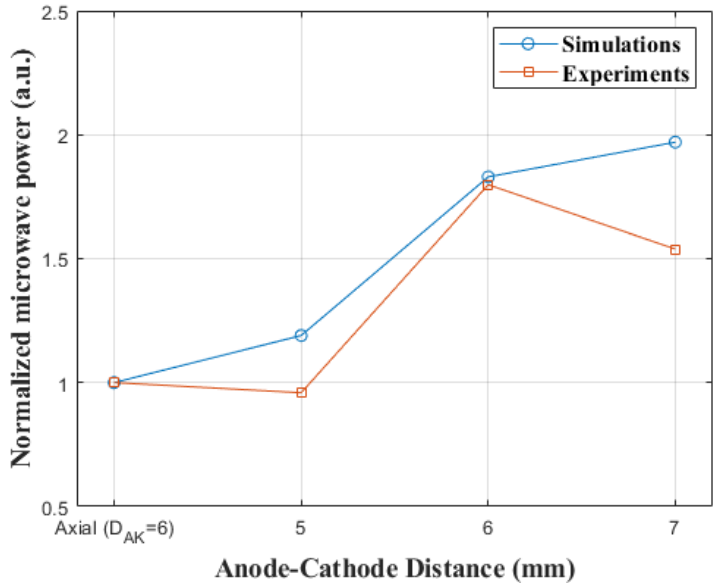

Figure 11. Normalized microwave power of the simulations and experiments as a function of the anode to cathode distance.

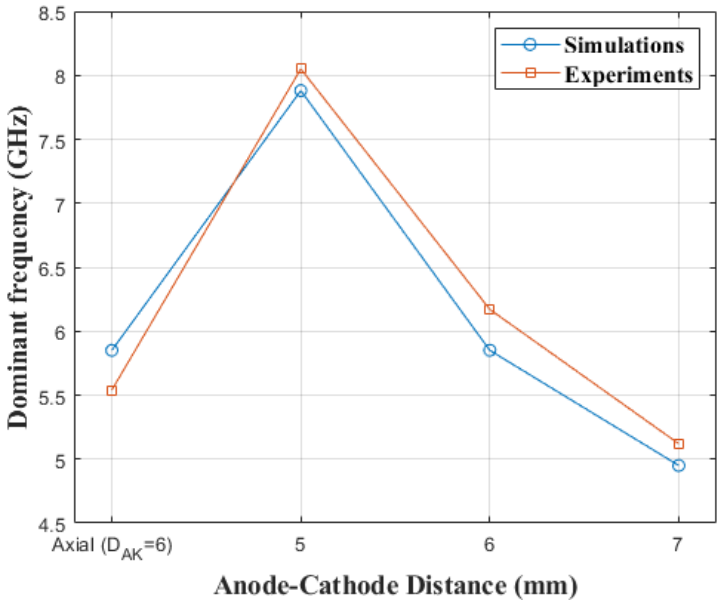

Figure 12. Dominant frequency of the simulations and experiments as a function of the anode to ring reflector distance.

4. Conclusions

The operation features of the coaxial vircator emitting electrons in the outer radial directions were investigated using PIC simulations experiments. The output microwave power and frequency of the proposed coaxial vircator were measured and compared with the simulation results. The operation features of the proposed coaxial vircator were compared with that of the axial vircator with the same anode to cathode distance (D_{AK} = 6 mm). The proposed coaxial vircator was also analyzed using the anode to cathode distances of 5 mm, 6 mm, and 7 mm. The vircator was operated using a −150 kV rectangular voltage pulse generated from a 10-stage PFN–Marx generator. The average value of the measured peak power and dominant frequency of the axial vircator was 11.22 MW and 5.54 GHz, respectively. When the proposed coaxial vircator was driven with the same anode to cathode distance, the average value of the peak power and dominant frequency

was 20.18 MW and 6.17 GHz. According to the simulations, the proposed coaxial cathode generates 83% more power than the axial vircator when the anode to cathode distance of both vircators is 6 mm. The experimental results on the vircators with the same anode to cathode distance show that the microwave power enhancement was 80%, which is in accordance with the simulation expectations. The proposed coaxial vircator enhances the microwave power dramatically when the anode to cathode distance is larger than 6 mm. The simulations and experiments show that the dominant frequency of the proposed coaxial vircator decreases inversely proportional to the anode to cathode distance, as observed in the axial vircator and normal coaxial vircator. Additionally, the proposed coaxial vircator has increasing tendencies proportional to the anode to cathode distance. The slight difference in the simulation and experimental results on the microwave power and the frequency is considered because of the misalignment, matching conditions between the vircator diode and pulsed power source, and crumpled condition of the mesh anode. The axial vircator and proposed coaxial vircator have different geometric factors that affect the operation features of the vircator. The geometric factors are affected by the electron beam shapes. Unlike the basic axial vircator with a solid or annular beam, the proposed coaxial vircator has more complex electron beam trajectories. In addition, because the experimental settings are not perfectly matched to the simulation setup, the geometric factors of the experiments can be slightly varied. This makes the geometric factors of the proposed coaxial vircator hard to analyze and causes a reduction in the accuracy of the simulation results. As future experiments, we intend to investigate the geometric factor of the coaxial vircator emitting electrons in the outer radial direction by changing the parameters of the vircator diode, such as the cathode radius, cathode length, and anode length.

Author Contributions: Conceptualization, S.-H.K. and C.-J.L.; methodology, S.-H.K., C.-J.L. and W.-I.K.; software, S.-H.K.; validation, S.-H.K., C.-J.L. and W.-I.K.; formal analysis, S.-H.K., C.-J.L. and W.-I.K.; investigation, S.-H.K., C.-J.L. and W.-I.K.; resources, S.-H.K.; data curation, S.-H.K.; writing—original draft preparation, S.-H.K.; writing—review and editing, K.-C.K. All authors have read and agreed to the published version of the manuscript.

Funding: This research received no external funding.

Data Availability Statement: Not applicable.

Conflicts of Interest: The authors declare no conflict of interest.

Abbreviations

The followings abbreviations are used in this manuscript.

HPM	High-Power Microwave
Vircator	VIRtual CAthode scillaTOR
PFN	Pulse-Forming Network
PEEK	Poly-Ether-Ether Ketone
FFT	Fast Fourier Transform
FDTD-PIC	Finite Difference Time Domain—Particle In Cell

References

1. Benford, J.; Swegle, J.A.; Schamiloglu, E. *High Power Microwaves*, 3rd ed.; CRC Press: Boca Raton, FL, USA, 2015.
2. Liu, Z.; Huang, H.; Jin, X.; Lei, L. Design of an X-Band Gigawatt Multibeam Relativistic Klystron Amplifier. *IEEE Trans. Plasma Sci.* **2014**, *42*, 3419–3422. [CrossRef]
3. Abubakirov, E.B.; Konyushkov, A.P.; Leontyev, A.N.; Rozental, R.M.; Tarakanov, V.P. Multi-pass relativistic traveling-wave tube with simultaneous operation on symmetric and asymmetric modes. *Phys. Plasmas* **2019**, *27*, 073104. [CrossRef]
4. Andreev, D.; Kuskov, A.; Schamiloglu, E. Review of the relativistic magnetron. *Matter Radiat. Extrem.* **2019**, *4*, 067201. [CrossRef]
5. Kumar, N.; Bera, A. RF Behavior of a Coaxial Interaction Structure for 0.24-Thz, 2-MW Gyrotron. *IEEE Trans. Electron Devices* **2020**, *67*, 3369–3377. [CrossRef]
6. Jiang, W.; Kristiansen, M. Theory of the virtual cathode oscillator. *Phys. Plasmas* **2001**, *8*, 3781–3787. [CrossRef]

7. Verma, R.; Shukla, R.; Sharma, S.K.; Banerjee, P.; Das, R.; Deb, P.; Prabaharan, T.; Das, B.; Mishra, E.; Adhikary, B.; et al. Characterization of High Power Microwave Radiation by an Axially Extracted Vircator. *IEEE Trans. Electron Devices* **2014**, *61*, 141–146. [CrossRef]
8. Jeon, W.; Lim, J.E.; Moon, M.W.; Jung, K.B.; Park, W.B.; Shin, H.M.; Seo, Y.; Choi, E.H. Output Characteristics of High-Power Microwave Generated From a Coaxial Vircator with a Bar Reflector in a Drift Region. *IEEE Trans. Plasma Sci.* **2006**, *34*, 937–944. [CrossRef]
9. Baryshevsky, V.; Gurinovich, A.; Gurnevich, E.; Molchanov, P. Experimental Study of an Axial Vircator with Resonant Cavity. *IEEE Trans. Plasma Sci.* **2015**, *43*, 3507–3511. [CrossRef]
10. Mumtaz, S.; Lim, J.S.; Ghimire, B.; Lee, S.W.; Choi, J.J.; Choi, E.H. Enhancing the power of high power microwaves by using zone plate and investigations for the position of virtual cathode inside the drift tube. *Phys. Plasmas* **2018**, *25*, 103113. [CrossRef]
11. Frolov, N.S.; Kurkin, S.A.; Koronovskii, A.A.; Hramov, A.E.; Rak, A.O. High-efficiency virtual cathode oscillator with photonic crystal. *Appl. Phys. Lett.* **2018**, *113*, 023503. [CrossRef]
12. Kim, S.-H.; Lee, C.-J.; Kim, W.-I.; Ko, K.-C. Experimental Investigation into the Optimum Position of a Ring Reflector for an Axial Virtual Cathode Oscillator. *Electronics* **2021**, *10*, 1878. [CrossRef]
13. Lie, L.; Hong, W.; Jun, Z.; Wen, J.-C.; Zhang, Y.-Z.; Liu, Y.-G. Fabrication of Carbon-Fiber Cathode for High-Power Microwave Applications. *IEEE Trans. Plasma Sci.* **2004**, *32*, 1742–1746. [CrossRef]
14. Li, L.; Liu, L.; Cheng, G.; Xu, Q.; Wan, H.; Chang, L.; Wen, J. The dependence of vircator oscillation mode on cathode material. *J. Appl. Phys.* **2009**, *105*, 123301. [CrossRef]
15. Menon, R.; Roy, A.; Singh, S.K.; Mitra, S.; Sharma, V.; Kumar, S.; Sharma, A.; Nagesh, K.V.; Mittal, K.C.; Chakravarthy, D.P. High power microwave generation from coaxial virtual cathode oscillator using graphite and velvet cathodes. *J. Appl. Phys.* **2010**, *107*, 093301. [CrossRef]
16. Rocha, E.; Kelly, P.M.; Parson, J.M.; Lynn, C.F.; Dickens, J.C.; Neuber, A.A.; Mankowski, J.J.; Queller, T.; Gleizer, J.; Krasik, Y.E. Evaluating the Performance of a Carbon-Epoxy Capillary Cathode and Carbon Fiber Cathode in a Sealed-Tube Vircator Under UHV Conditions. *IEEE Trans. Plasma Sci.* **2015**, *43*, 2670–2675. [CrossRef]
17. Jiang, W.; Woolverton, K.; Dickens, J.; Kristiansen, M. High Power Microwave Generation by a Coaxial Virtual Cathode Oscillator. *IEEE Trans. Plasma Sci.* **1999**, *27*, 1538–1542. [CrossRef]
18. Chen, X.; Toh, W.K.; Lindsay, P.A. Physics of the Interaction Process in a Typical Coaxial Virtual Cathode Oscillator Based on Computer Modeling Using MAGIC. *IEEE Trans. Plasma Sci.* **2004**, *32*, 1191–1199. [CrossRef]
19. Chen, X.; Dickens, J.; Mankowski, J.; Hatfield, L.L.; Choi, E.H.; Kristiansen, M. Microwave Frequency Determination Mechanisms in a Coaxial Vircator. *IEEE Trans. Plasma Sci.* **2004**, *32*, 1799–1804. [CrossRef]
20. Sung, K.Y.; Jeon, W.; Jung, Y.; Lim, J.E.; Uhm, H.S.; Choi, E.H. Influence of Anode-Cathode Gap Distance on Output Characteristics of High-Power Microwave From Coaxial Virtual Cathode Oscillator. *IEEE Trans. Plasma Sci.* **2005**, *33*, 1353–1357. [CrossRef]
21. Shao, H.; Liu, G.; Yang, Z.; Chen, C.; Song, Z.; Huang, W. Characterization of Modes in Coaxial Vircator. *IEEE Trans. Plasma Sci.* **2006**, *34*, 7–13. [CrossRef]
22. Xing, Q.; Wang, D.; Huang, F.; Deng, J. Two-Dimensional Theoretical Analysis of the Dominant Frequency in the Inward-Emitting Coaxial Vircator. *IEEE Trans. Plasma Sci.* **2006**, *34*, 584–589. [CrossRef]
23. Moller, C.; Elfsberg, M.; Hurtig, T.; Larsson, A.; Nyholm, S.E. Proof of Principle Experiments on Direct Generation of the TE_{11} Mode in a Coaxial Vircator. *IEEE Trans. Plasma Sci.* **2010**, *38*, 26–31. [CrossRef]
24. Biswas, D.; Kumar, R. Microwave Power Enhancement in the Simulation of a Resonant Coaxial Vircator. *IEEE Trans. Plasma Sci.* **2010**, *38*, 1313–1317. [CrossRef]
25. Zhang, Y.; Liu, G.; Shao, H.; Liang, T.; Zhang, L.; Teng, Y.; Yan, L.; Lin, Y. Numerical and Experimental Studies on Frequency Characteristics of TE_{11}-Mode Enhanced Coaxial Vircator. *IEEE Trans. Plasma Sci.* **2011**, *39*, 1762–1767. [CrossRef]
26. Roy, A.; Menon, R.; Mitra, S.; Sharma, A.; Nagesh, K.V.; Chakravarthy, D.P. Influence of Electron-Beam Diode Voltage and Current on Coaxial Vircator. *IEEE Trans. Plasma Sci.* **2012**, *40*, 1601–1606. [CrossRef]
27. Andersson, J.; Sansson, M.; Aberg, D. Frequency Dependence of the Anode-Cathode Gap Spacing in a Coaxial Vircator System. *IEEE Trans. Plasma Sci.* **2013**, *41*, 2758–2762. [CrossRef]
28. Turner, G.R. A one-dimensional model illustrating virtual-cathode formation in a novel coaxial virtual-cathode oscillator. *Phys. Plasmas* **2014**, *21*, 093104. [CrossRef]
29. Barnett, D.H.; Rainwater, K.; Dickens, J.C.; Neuber, A.A.; Mankowski, J.J. A Reflex Triode System with Multicavity Adjustment. *IEEE Trans. Plasma Sci.* **2019**, *47*, 1472–1476. [CrossRef]
30. Zhang, H.; Shu, T.; Liu, S.; Zhang, Z.; Song, L.; Zhan, H. A Compact Modular 5 GW Pulse PFN-Marx Generatro for Driving HPM Source. *Electronics* **2021**, *10*, 545. [CrossRef]
31. Zhang, H.; Yang, J.; Lin, J.; Yang, X. A compact bipolar pulse-forming network-Marx generator based on pulse transformers. *Rev. Sci. Instrum.* **2013**, *84*, 114705. [CrossRef] [PubMed]
32. Song, K.B.; Lim, J.E.; Seo, Y.; Choi, E.H. Output Characteristics of the Axially Extracted Virtual Cathode Oscillator with a Cathode-Wing. *IEEE Trans. Plasma Sci.* **2009**, *37*, 304–310. [CrossRef]